Results in Engineering 25 (2025) 104312

Contents lists available at ScienceDirect

Results in Engineering

journal homepage: www.sciencedirect.com/journal/results-in-engineering

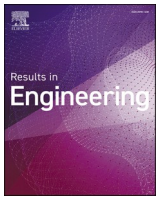

Research paper

Modified polyvinylidene fluoride membranes for effective removal of iron ions (Fe^{2+}) from water

Halyna Bubela [a,*], Viktoriia Konovalova [a], Joanna Kujawa [b], Wojciech Kujawski [b,*]

[a] Department of Chemistry, National University of Kyiv-Mohyla Academy, 2 Skovoroda Street, 04070 Kyiv, Ukraine
[b] Nicolaus Copernicus University in Toruń, Faculty of Chemistry, 7 Gagarina Street, 87-100 Toruń, Poland

ARTICLE INFO

Keywords:
PVDF membrane
Membrane surface modification
Fe_3O_4 nanoparticles
Magnetically active membranes
Fe^{2+} removal

ABSTRACT

Paper introduces an efficient technique for removing excess Fe(II) ions from water using modified polyvinylidene fluoride membranes. Capability for Fe(II) removal was investigated for three types of PVDF membranes (pristine PVDF, PVDF/Fe_3O_4 blend, and PVDF/Fe_3O_4 blend membrane with additional immobilization of Fe_3O_4 nanoparticles using polymer spacer. Structures and morphologies of membranes were analyzed through various techniques (IR, SEM, AFM, water contact angle, zeta potential), revealing that Fe_3O_4 nanoparticles were successfully incorporated into the membrane matrix and/or the membrane surface. The surface modification resulted in increased hydrophilicity of the membrane surface, as indicated by a decrease of WCA from 106.1°±3° to 74.8°±2°. The isoelectric point changed from 3.5 ± 0.2 to 7.9 ± 0.2 after the attachment of polyethyleneimine (PEI) owing to the cationic nature of the polymer linker. Membranes were tested in an ultrafiltration process using polyacrylic acid (PAA) as an agent for the binding of Fe(II) into the coordination complex. The modified membranes demonstrated a hydrodynamic permeability coefficient of 17.1 LMH·bar^{-1}, which is approximately 2.5 times higher than the pristine PVDF membrane. The surface-modified PVDF membranes maintained a high rejection of Fe(II)-PAA coordination complex (97.1 and 99.4 %, respectively) at a pH of 8, leading to the decrease of concentration of Fe(II) in permeate from 20 ppm to 0.08 ppm and 0.11 ppm, meeting the standards set by the World Health Organization (0.3 ppm) and European Union Regulation (0.2 ppm). Modified PVDF/Fe_3O_4 membranes show potential applications in water purification from heavy metals owing to many advantages, including higher flux rates and rejection ability.

1. Introduction

Iron (Fe) is a vital element which plays a key role in the metabolism of living organisms, including humans [1]. Iron is a heavy metal naturally found in the earth's crust. The presence of iron in water, typically in the soluble ferric or insoluble ferrous forms, can result from the dissolution of rocks and minerals, as well as from acid mine drainage or industrial waste [2,3]. However, an excess of iron content in drinking water may cause a problem owing to harmful effects on human health (e.g., diabetes, hemochromatosis, stomach problems, and nausea) [4]. Moreover, ferrous sulfate has the ability to settle out as corrosion colored silt, causing an undesirable metallic taste in water and damaging of pipes [5]. Considering these facts, the World Health Organization (WHO) suggests the content of iron should be lower than 0.3 ppm [6]; furthermore, the European Union Regulations propose an iron concentration limit of 0.2 ppm [7].

Owing to the fact that groundwaters may contain iron at concentrations of up to several milligrams per liter, it is important to develop an inexpensive, convenient, and reliable method to purify water to the required iron concentration [8–10]. PVDF membranes are one of the most common polymeric membranes owing to their low-price chemical stability and mechanical resistance [11,12]. PVDF membranes and their modified derivatives are widely used to remove metal ions in the water purification process [13–16]. Zhao et al. [17] fabricated a MoS_2 nanosheet functionalized PVDF membrane to remove mercury (II) ions. Removal capability, adsorption rate, and the removal mechanism of Hg^{2+} ions were investigated. It was revealed that a high Hg^{2+} ions removal efficiency of over 99 %, even from oil-field wastewater, can be reached. Therefore, the PVDF membranes with MoS_2 demonstrated the potential application for industrial wastewater purification from heavy metal ions. Teng et al. [18] developed PVDF membranes coated with polyethyleneimine (PEI) and epoxidized SiO_2 nanoparticles with heavy

* Corresponding authors.
E-mail addresses: halyna.bubela@ukma.edu.ua (H. Bubela), wkujawski@umk.pl (W. Kujawski).

https://doi.org/10.1016/j.rineng.2025.104312
Received 28 November 2024; Received in revised form 28 January 2025; Accepted 6 February 2025
Available online 7 February 2025

Table 1
Labeling of the investigated membranes.

Membrane	Initial evaporation time [min]	Label
PVDF	0	PVDF
PVDF	10	PVDF 10
PVDF doped with Fe_3O_4	0	PVDF/Fe_3O_4
PVDF doped with Fe_3O_4	10	PVDF/Fe_3O_4 10
PVDF/Fe_3O_4 with subsequent surface modification	0	S-PVDF/ Fe_3O_4
PVDF/Fe_3O_4 with subsequent surface modification	10	S-PVDF/ Fe_3O_4 10

metal ions removal capabilities. Cd^{2+}, Cu^{2+}, and Pb^{2+} were chosen as representatives to evaluate the ability of such membranes to remove heavy metal ions. It was determined that the rejection coefficients of Cd^{2+}, Cu^{2+}, and Pb^{2+} ions were 79.2 ± 1.7 %, 74.2 ± 1.9 %, and 76.4 ± 1.9 %, respectively. Pirashmani et al. [19] fabricated PVDF nanofibrous ultrafiltration (UF) membranes modified with metal-organic framework nanoparticles, including ZIF-8, chitosan/UiO-66 NH_2, and chitosan/ZIF-8. The removal performance of the membranes was assessed in the UF process with BSA protein and Cr^{6+} ions. The PVDF/chitosan membrane loaded with UiO-66-NH_2 (20 wt %) demonstrated the highest water flux of 470 LMH, along with BSA and Cr^{6+} rejection rates of 98.1 % and 95.6 %, respectively.

Nevertheless, the inherent hydrophobicity of PVDF leads to surface fouling [20], which raises the operational costs associated with PVDF filters, making their use in water treatment unaffordable in resource-constrained settings [21,22]. Volumetric, physical, and chemical modification can be used to achieve the required characteristics of PVDF membranes for specific separation processes [23,24]. The volumetric method signifies adding supplements to the polymer solution during the formation process [25,26].

Physical modification is usually presented as coating with high molecular weight substances, oligomers, and surfactants, and is based on ionic or hydrophobic interactions [27–30]. A chemical modification process is applied to enhance the membrane susceptibility to fouling and allows the immobilization of other molecules on the membrane surface owing to new covalently bound molecules with reactive functional groups [31–33]. However, PVDF membranes possess inert properties, and pre-activation treatment is required [34–36].

The volumetric modification of PVDF membranes using magnetite (Fe_3O_4) nanoparticles (MNPs) to enhance microstructure, reduce fouling, and enable smart functionalities has been extensively studied in the literature [37–40]. Moreover, chemical modification methods with Fe_3O_4 nanoparticles greatly enhance membrane efficiency [41,42] owing to the mobility of MNPs in a magnetic field [43]. Applying iron (II, III) oxide expands the permeate water flux and minimizes the impact of concentration polarization and membrane fouling [44,45]. Considering these facts, the modification proposed by Himstedt et al. [46,47] is a promising approach to fabricating PVDF membranes with higher mass transfer values and salt rejection coefficients. Konovalova et al. [43] developed polyethersulfone membranes with immobilized magnetite nanoparticles and proved their improved transport properties in the UF process for polymers with different molecular mass.

In this work, polyvinylidene fluoride membranes were modified using both volumetric and chemical modifications. It is worth noting that such dual approach has not been previously described in the literature. The applicability of PVDF membranes for iron (II) removal applying the polyelectrolyte-enhanced UF was investigated. Three types of PVDF membranes (pristine PVDF, PVDF doped with Fe_3O_4, and PVDF/Fe_3O_4 with subsequent immobilization of Fe_3O_4 nanoparticles

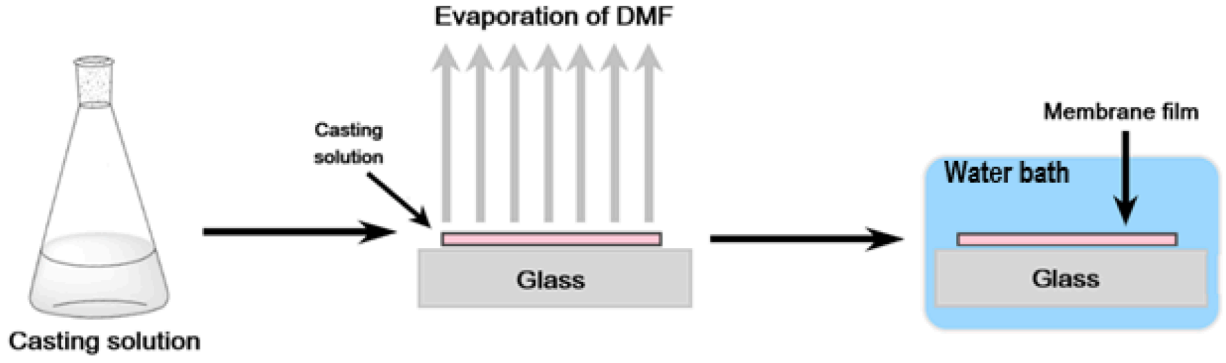

Fig. 1. Schematic depiction of the membrane formation using a phase inversion method induced by a nonsolvent, with initial evaporation stage.

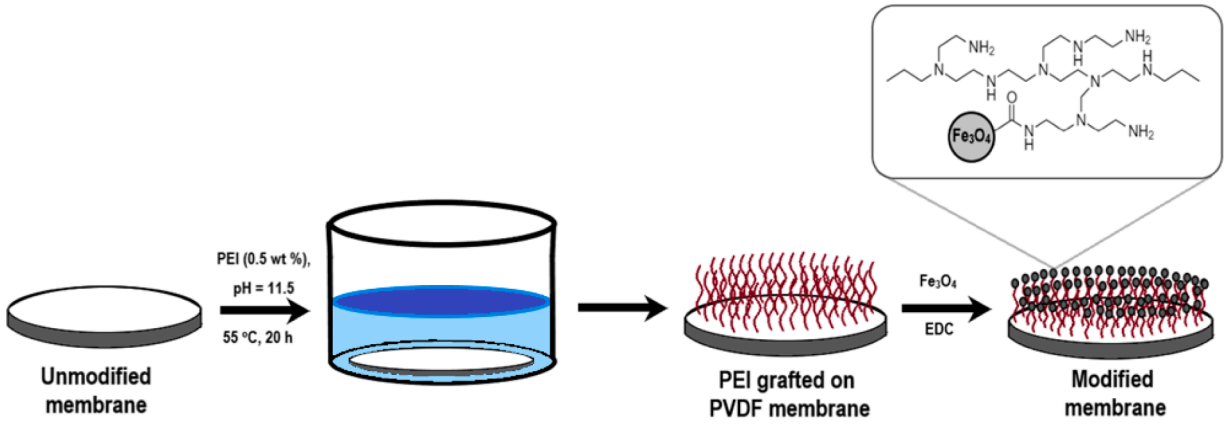

Fig. 2. Schematic depiction of surface modification of PVDF/Fe_3O_4.

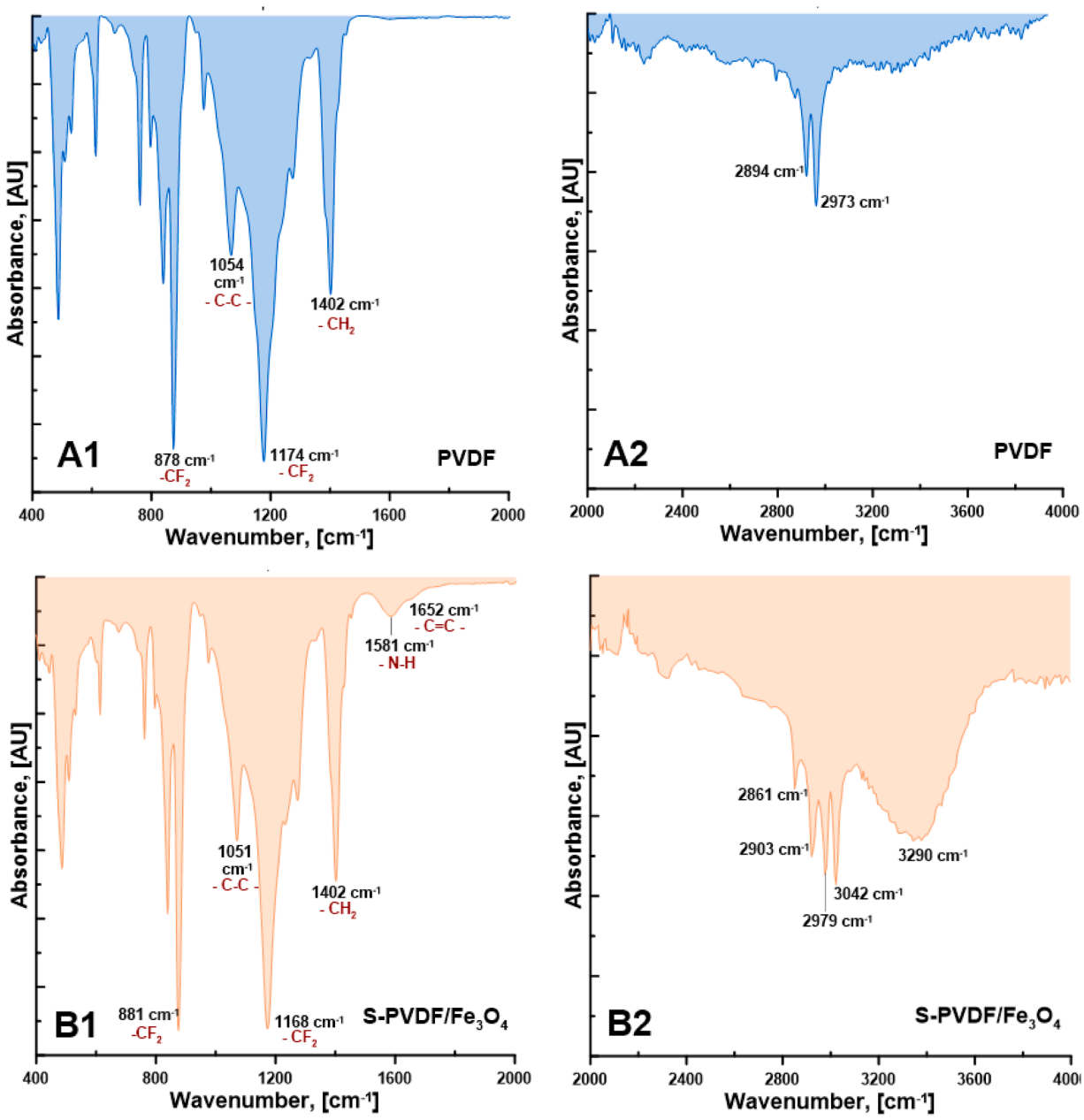

Fig. 3. FTIR spectra of pristine PVDF (A1, A2), and modified (B1; B2) PVDF membranes.

with PEI as a polymer linker) were fabricated, and their surface, morphological, and transport properties were analyzed. The essential goal was to develop and utilize PVDF membranes to effectively purify water to the iron level suggested by the European Union Regulation (0.02 ppm). Therefore, the transport and separation properties were evaluated using the ultrafiltration process. The iron (II) ions were bound into a complex with polyacrylic acid (PAA) for effective purification. Moreover, the influence of PAA and pH value of feed were studied.

2. Materials and methods

2.1. Materials

Polyvinylidene fluoride powder KYNAR HSV900 (Arkema, France) was used for the membrane fabrication with N,N-Dimethylformamide (DMF) (Chempur, Poland) serving as the organic solvent to prepare the PVDF solution.

The following chemicals were utilized in the modification process: Na_2CO_3 (Chempur, Poland), 25 kDa PEI (Sigma-Aldrich Co, USA), Fe_3O_4 nanoparticles with particle size of 50 nm (Sigma-Aldrich Co, USA), 5.1 kDa polyacrylic acid sodium salt (PAASS) (Sigma-Aldrich Co, USA), 1-ethyl-3-(3-dimethylaminopropyl) carbodiimide (EDC) (Sigma-Aldrich Co, USA).

2.2. Membrane formation

To fabricate membranes by the phase inversion method, two casting solutions were prepared (Table 1): (1) 15 wt % PVDF in DMF without iron (II, III) oxide nanoparticles for membranes, subsequently labeled as PVDF and (2) 15 wt % PVDF and 1 wt % Fe_3O_4 nanoparticles in DMF for PVDF/Fe_3O_4. Each solution was stirred overnight to ensure a homogeneous mixture. Subsequently, the degassing (1 h), and maturing stages (24 h) were performed.

An automatic film applicator (Erichsen Gmbh Co., Germany) with a

Table 2
Results of thickness measurement and water uptake values for investigated PVDF membranes.

Membrane	IET, [min]	Thickness, [μm]		Thickness change, [%]	Water uptake, [%]
		Wet membrane	Dry membrane		
PVDF	0	44 ± 1	41 ± 1	7.3 ± 1	10.5 ± 3.1
PVDF	10	60 ± 3	52 ± 3	15.4 ± 1	14.7 ± 2.9
PVDF/Fe_3O_4	0	55 ± 3	43 ± 2	21.9 ± 1	18.8 ± 3.1
PVDF/Fe_3O_4	10	83 ± 3	66 ± 3	25.8 ± 1	24.8 ± 3.0
S-PVDF/Fe_3O_4	0	60 ± 3	44 ± 2	36.3 ± 1	37.4 ± 3.4
S-PVDF/Fe_3O_4	10	91 ± 4	68 ± 3	33.8 ± 1	35.6 ± 3.8

casting speed of 10 mm·s^{-1} was used to prepare membrane films. The dope solution was poured onto a glass plate, and after that, a casting knife with a slit thickness of 0.4 mm was used to form the membranes (Fig. 1) [48]. Polymer solutions were kept for a specified time (0 and 10 min) called initial evaporation time (IET). Afterward, the glass plate with the dope solution was submerged in a coagulation bath filled with deionized water for 20 min. To remove the excess amount of solvent, membranes were placed in DI water for 24 h.

2.3. Membrane modification

The surface modification technique was thoroughly outlined in our previous work [49]. In brief, a simple modification method was used to develop the Fe_3O_4-decorated membrane, as shown in Fig. 2. The essential idea was to immobilize MNPs with PEI as a linker between the activated membrane surface and the functionalized magnetite. Owing to the inertness of the PVDF, the activation step using carbonate buffer firstly was carried out [50,51]. As a consequence, the defluorination process and the formation of double bonds occurred. Next, PEI was grafted onto the membrane through nucleophilic substitution, where the amino groups of PEI replaced the fluorine on sp^2-hybridized carbon. Afterward, the attachment of MNPs occurred via an amide bond between amino groups of polyethyleneimine and carboxylic groups of functionalized Fe_3O_4 nanoparticles. EDC was used as an activator of the amidation reaction [49].

2.4. Membrane characterization

FTIR spectroscopy was utilized to prove a successful modification process and to study the characteristic peaks of the PVDF, PVDF/Fe_3O_4, and S-PVDF/Fe_3O_4. All of the spectra were obtained for wavenumbers between 4000 cm^{-1} and 400 cm^{-1} using a FTIR spectrometer Bruker Vertex 80v (Billerica, Massachusetts, USA).

The thicknesses of membranes were measured using a micrometer (Sylvac, Switzerland). Samples were kept in an oven at 50 °C for 24 h and, after that, the thicknesses of the dry samples (T_{dry}) were determined. Measurements were performed at least 20 times for each sample. A similar experiment was carried out for wet membranes. The results for wet samples (T_{wet}) were acquired after keeping membranes in water for 24 h. Thickness change was calculated using Eq. (1).

$$\text{Thickness change } [\%] = \frac{T_{wet} - T_{dry}}{T_{dry}} 100\% \quad (1)$$

Water uptake (WU) was determined according to Eq. (2):

$$\text{WU } (\%) = \frac{m_{wet} - m_{dry}}{m_{dry}} 100\% \quad (2)$$

Before the evaluation, membrane samples were stored at 50 °C for 24 h. Subsequently, the samples were weighed and the masses of dry samples (m_{dry}) were measured. The masses of the wet membranes (m_{wet})

Table 3
Initial evaporation time (IET), water contact angle (WCA), and porosity values of investigated membranes.

Membrane	IET, [min]	Contact angle, [°]	Porosity, [%]
PVDF	0	106.1 ± 3.2	7.4 ± 2
PVDF	10	109.0 ± 3.6	15.6 ± 2
PVDF/Fe_3O_4	0	93.0 ± 3.8	11.5 ± 2
PVDF/Fe_3O_4	10	96.1 ± 3.1	19.6 ± 2
S-PVDF/Fe_3O_4	0	74.8 ± 3.7	10.4 ± 2
S-PVDF/Fe_3O_4	10	76.1 ± 3.8	17.9 ± 2

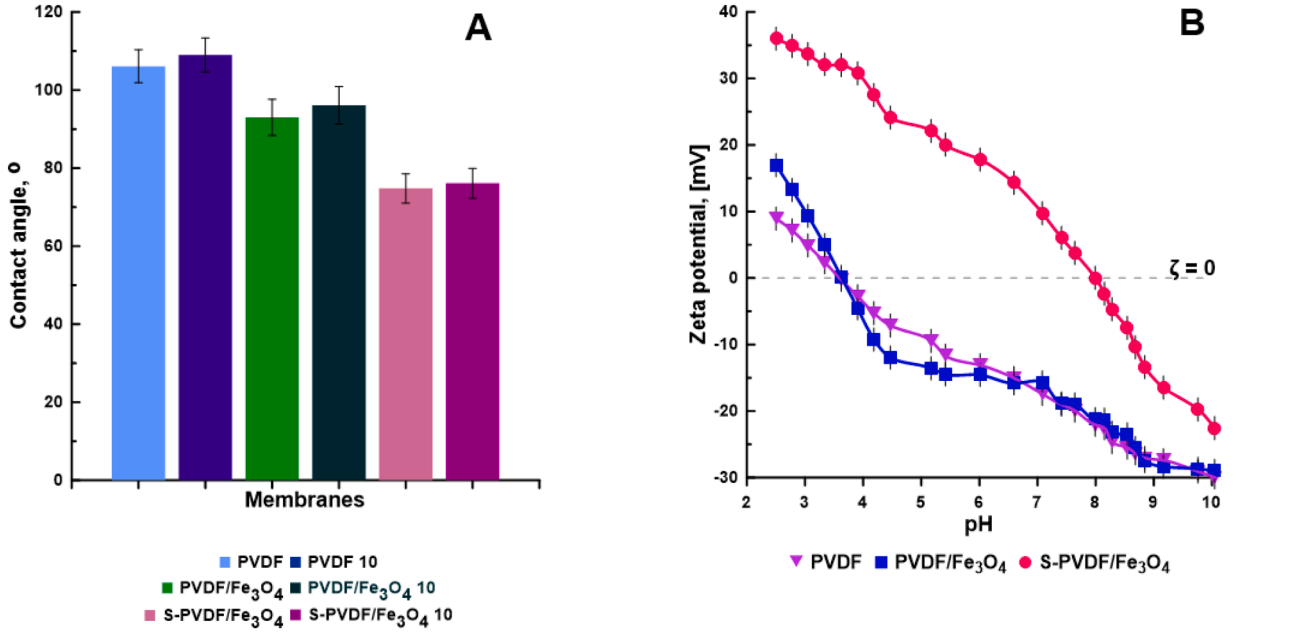

Fig. 4. WCA (A) and zeta potential analyzes (B) in the pH range 2–10.

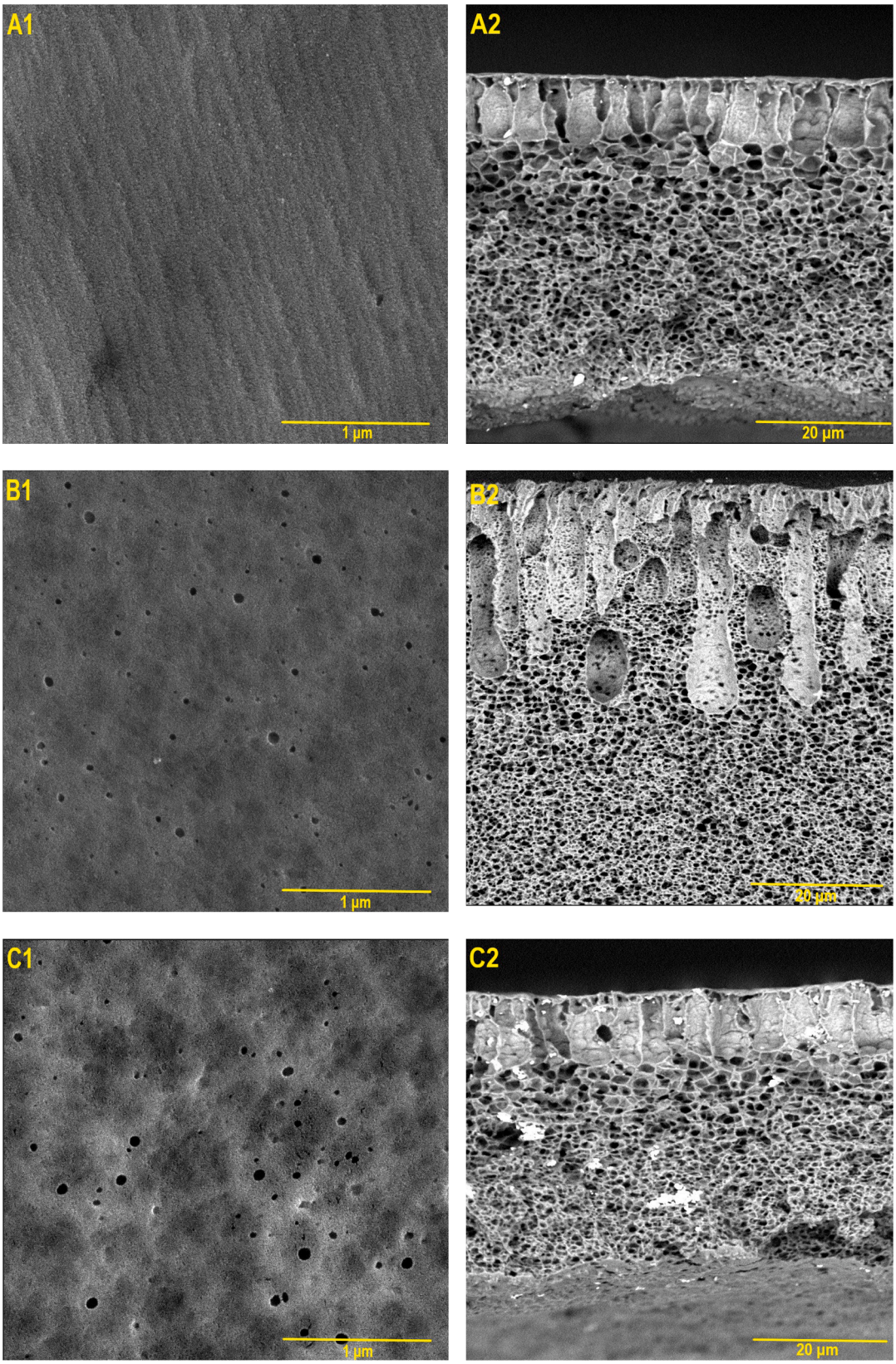

Fig. 5. Top and cross-sectional microphotographs of: (A1, A2) – PVDF; (B1, B2) – PVDF 10; (C1, C2) – PVDF/Fe_3O_4; (D1, D2) – PVDF/Fe_3O_4 10; (E1, E2) – S-PVDF/Fe_3O_4; (F1, F2) – S-PVDF/Fe_3O_4 10.

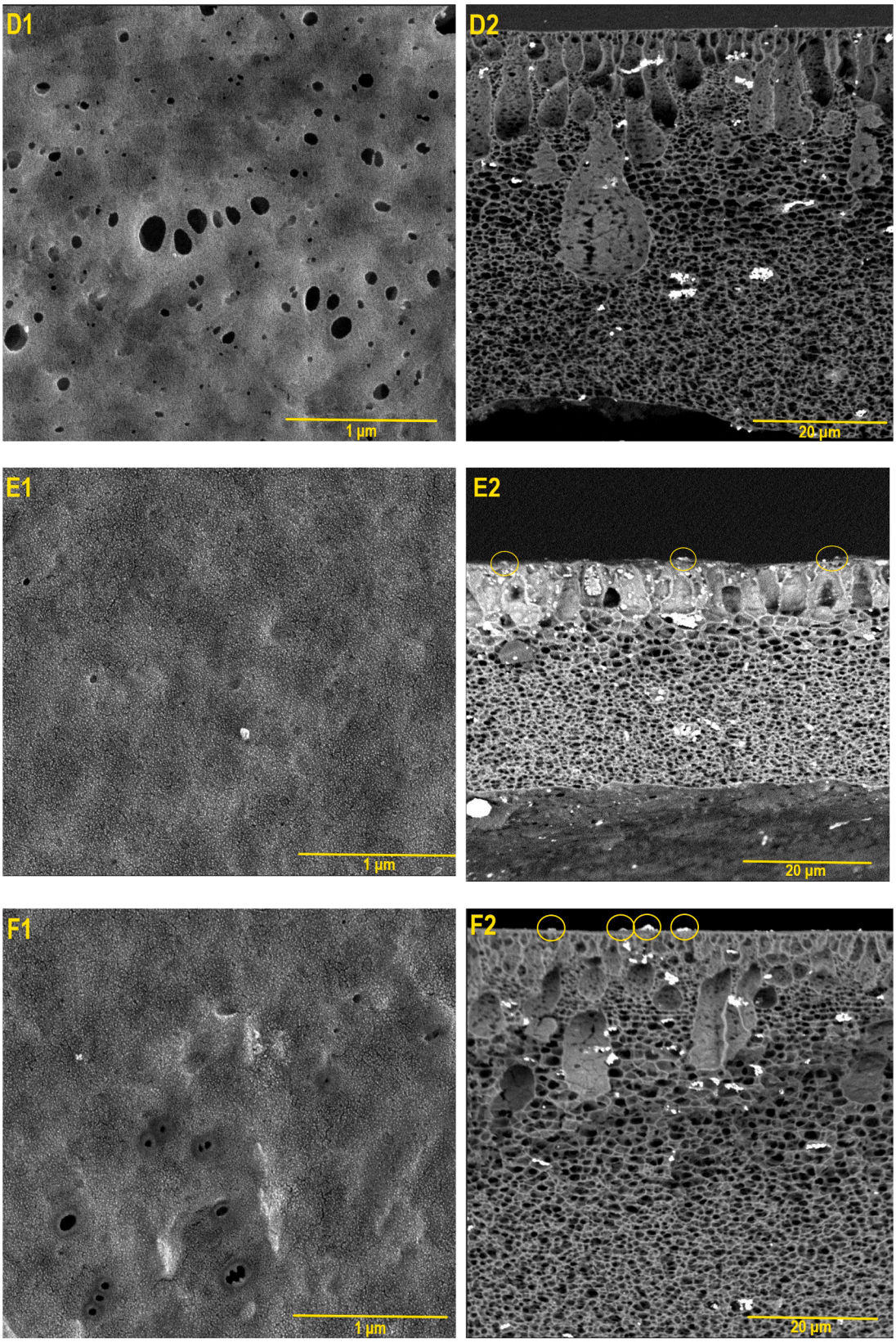

Fig. 5. (*continued*).

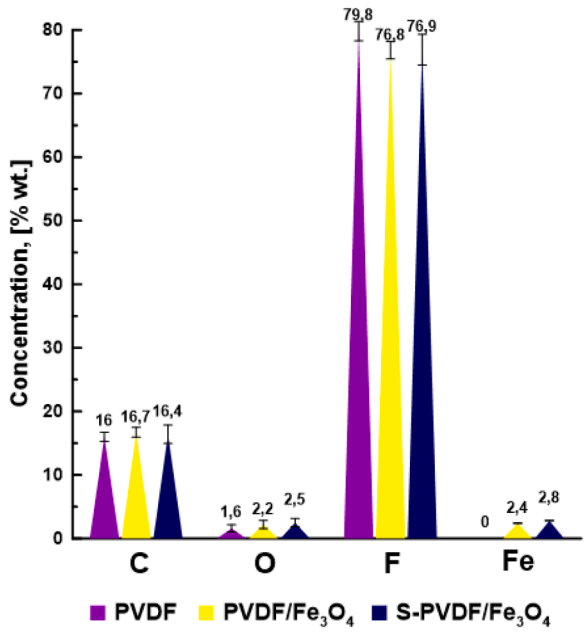

Fig. 6. Results of EDX analysis for PVDF, PVDF/Fe_3O_4, and S-PVDF/Fe_3O_4.

were estimated after placing samples in deionized water for 24 h. An experiment for each sample was conducted three times, and average values were presented. Based on the results of water uptake experiments, the volume porosity was calculated according to Eq. (3):

$$\text{Porosity } (\%) = \varepsilon\ (\%) = \frac{m_{wet} - m_{dry}}{Q_{water} * A * L} 100\% \quad (3)$$

where m_{wet} – mass of wet membranes, kg; m_{dry} – mass of dry membranes, kg; Q – water density, kg·m^{-3}; A – membrane surface area, m^2; L – membrane thickness, m.

To evaluate the dependence of zeta potential from pH, Surpass3 electrokinetic analyzer (Anton Paar, Austria) was employed. To assess the hydrophilicity/hydrophobicity properties of the membranes, goniometric studies were conducted using a goniometer (Biolin Scientific Gothenburg, Sweden). Contact angle values were determined for water ($\gamma = 72.7$ mN m^{-1}) with a drop volume of 3 μL. Each measurement was repeated 10 times at room temperature, and average values were calculated.

The top surface and cross-section microstructural images of the membrane samples were acquired using a scanning electron microscope (SEM), Quanta 3D FEG (FEI, Prague, Czech Republic). To improve the visibility of macrophotographs, the membrane samples were coated with a gold nanolayer (thickness of ca. 1 nm) before the experiments. For cross-sectional images, samples were prepared by freezing and fracturing the membranes in liquid nitrogen. EDX analysis of cross-section was carried out with the aim of elemental analyzes; the EDX experiment was performed utilizing an energy-dispersive X-ray system with SEM.

Average roughness and root mean square roughness (RMS) are important parameters characterizing the surface morphology of the samples. An atomic force microscope (AFM), (Veeco, Digital Instrument, United Kingdom), was used to evaluate the RMS parameter; the investigated area was 10 μm x 10 μm. The results of AFM experiments were explored with NanoScope Analysis Software (1.40, Build R3Sr5.96909, 2013 Bruker Corporation).

The transport characteristics of membranes were investigated using a dead-end ultrafiltration setup characterized by an effective membrane area of 12.56 cm^2. Analyzes were performed at room temperature, applying pressures ranging from 0.5 to 2.5 bar. A Janke Kunkel KMO_2 magnetic stirrer was employed to create a magnetic field and stirring in time of UF (stirring rate 250 rpm). To verify the obtained flux values, every experiment was repeated 3 times. Besides, before each measurement, the membrane was compacted with deionized water for 2 h at a pressure of 3 bar to achieve a stable flux. Then, pure water was filtrated through the membrane for 1 h and the average water flux (Jv, LMH) was calculated using Eq. (4), where ΔV corresponds to the permeate volume (L), Δt is the time for filtrate to pass through the membrane (h), A is the active membrane area (m^2). Membrane hydrodynamic permeability coefficient (Lp, LMH·bar^{-1}) is determined as a slope of dependence of Jv on the applied pressure (Δ p) [52].

$$Jv = \frac{\Delta V}{A\ \Delta t} \quad (4)$$

The same experiment was conducted to assess the ability of membranes to retain iron ions Fe^{2+} through polyelectrolyte-enhanced UF. Before this, the membranes were characterized using organic tracer filtration experiments [53]. Polyethylene glycols (PEG) with different molecular weights (4 kDa, 8 kDa, and 20 kDa) were employed as tracers. The results showed retention values of 100 % for PEG 8 kDa and PEG 20 kDa, while PEG 4 kDa exhibited a retention of approximately 85 %. Based on these findings, PAASS of 5.1 kDa was selected to bind Fe^{2+} ions into a complex for their removal via polyelectrolyte-enhanced ultrafiltration.

Ammonium iron (II) sulfate hexahydrate $(NH_4)_2Fe(SO_4)_2$ was used to prepare a feed solution with Fe^{2+} concentration of 20 mg·L^{-1}.PAASS was added to the solution (concentration 0.1 wt %, 0.3 wt %, 0.5 wt %) to bind Fe^{2+} ions into the complex with carboxyl acid groups. UF experiments for Fe^{2+}-PAA water solutions were performed at pH of 4, 6, and 8, with an initial feed volume of 50 mL. The rejection rate was calculated when the recovery reached 50 %. The concentrations of Fe^{2+} were determined by the atomic absorption spectrometer SOLAAR 969. Rejection (R, %) values were evaluated via Eqs. 5, where C_p and C_f denote the Fe^{2+} ions concentrations in the permeate and feed solutions, respectively [54].

$$R = 1 - \left(\frac{C_p}{C_f}\right) 100\% \quad (5)$$

3. Results and discussion

3.1. FTIR spectroscopy

To confirm the membrane modification, FTIR spectroscopy was utilized for the assessment of the functional groups and chemical composition of the pristine PVDF, and the modified PVDF membranes (Fig. 3). Some similar peaks were observed in the spectra of all the samples, a fact which is obviously related to the characteristic peaks of the PVDF membrane. The peaks at 878 cm^{-1} and 1174 cm^{-1} corresponded to CF_2 stretching; the peak at 1054 cm^{-1} was characteristic for the C–H range of -CH_2F of alkyl halides; and at 1402 cm^{-1} was attributed to the CH_2 group.

The activation of the surface by carbonate buffer with subsequent grafting of PEI makes it possible to produce the amino groups on the PVDF surface. In the spectrum of S-PVDF/Fe_3O_4 membrane, the characteristic broad band of amino moieties at 3100–3500 cm^{-1} was clearly visible (Fig. 3, B1); moreover, the band at 1581 cm^{-1} corresponded to the deformation fluctuation of N-H bonds. In addition, the appearance of new bands at 3042 cm^{-1}, 2861 cm^{-1}, and 1652 cm^{-1} was related to the defluorination, double bond formation, and -CF substitution with -CH [55].

3.2. Membranes characterization

The results of thickness measurement and WU values for the investigated PVDF membranes are presented in Table 2. Thickness changes were calculated according to Eq. (1). As can be concluded from the

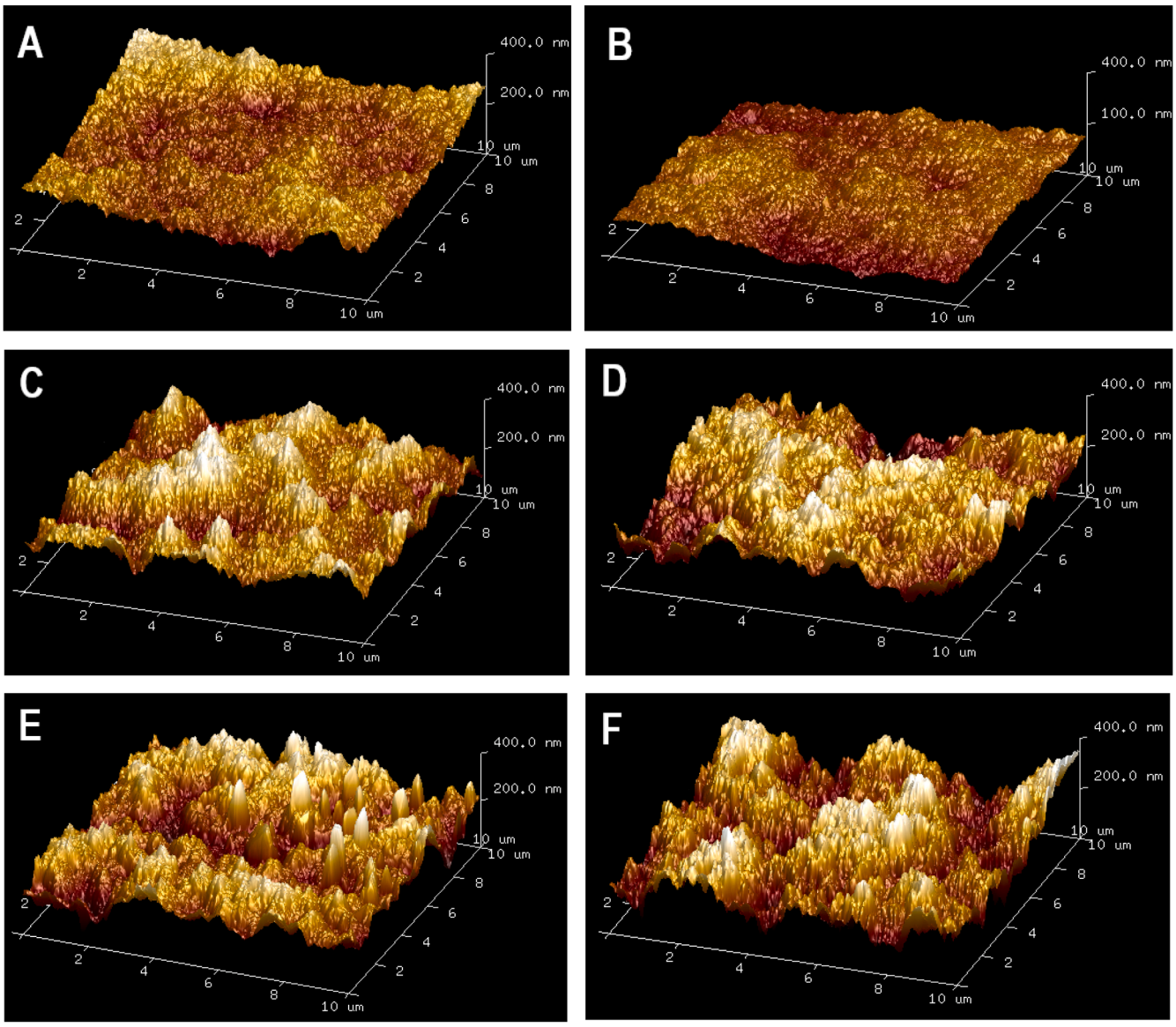

Fig. 7. 3D AFM images: (A) – PVDF; (B) – PVDF 10; (C) – PVDF/Fe_3O_4; (D) – PVDF/Fe_3O_4 10; (E) – S-PVDF/Fe_3O_4; (F) – S- PVDF/Fe_3O_4 10.

Table 4
Average roughness and RMS values of developed PVDF membranes.

Membrane	Average roughness, [nm]	RMS roughness, [nm]
PVDF	29.8 ± 0.3	26.7 ± 0.3
PVDF 10	34.1 ± 0.3	28.7 ± 0.3
PVDF/Fe_3O_4	36.2 ± 0.3	30.4 ± 0.3
PVDF/Fe_3O_4 10	36.8 ± 0.3	31.3 ± 0.3
S-PVDF/Fe_3O_4	43.7 ± 0.3	54.2 ± 0.3
S-PVDF/Fe_3O_4 10	41.8 ± 0.3	46.5 ± 0.3

presented values, the membrane thickness depends on the IET during the membrane formation process [48]. The thickness increased with extended initial evaporation time (41 ± 1.1 μm and 52 ± 3.0 μm for PVDF without and with IET of 10 min, respectively). Besides, the PVDF/Fe_3O_4 membranes were characterized by increased thickness values compared to the pristine PVDF (Table 2).

Water uptake values, calculated using Eq. (2), are shown in Table 2. It is interesting to notice that the increase of water uptake was observed for the PVDF membranes formed with Fe_3O_4 (10.5 ± 3.1 % *vs.* 18.8 ± 3.1 % for membranes without additional evaporation time, and 14.7 ± 2.9 % *vs.* 24.8 ± 3.0 % for membranes with IET of 10 min). This 44–47 % increase in WU suggests that the incorporation of magnetite nanoparticles into the PVDF membrane matrix enhanced the hydrophilicity of PVDF membranes. Increased hydrophilicity of PVDF/Fe_3O_4 membranes compared with original PVDF was also confirmed by the contact angle values (Fig. 4, Table 3). PVDF and PVDF/Fe_3O_4 membranes (without IET) possessed hydrophobic characteristics showing contact angles of 106° and 93° respectively. As for PVDF and PVDF/Fe_3O_4 membranes with IET of 10 min, contact angle values were equal to 109° and 96°, respectively. Obviously, the membranes with surface modification possessed a hydrophilic nature (WCA < 90°) with the lowest values of contact angles (74.8° and 76.1°) because PEI is a hydrophilic agent.

One of the important characteristics of membrane materials is their surface charge. A streaming potential analysis was performed to obtain more comprehensive information regarding the properties of developed membranes (Fig. 4B). A strong impact of surface modification on the surface properties was observed. PVDF and PVDF/Fe_3O_4 were characterized by the isoelectric point (IEP) of 3.5 ± 0.2 and 3.7 ± 0.2, respectively. The lack of significant shifts in IEP for PVDF, and PVDF/Fe_3O_4 indicates that the modification took place only inside the

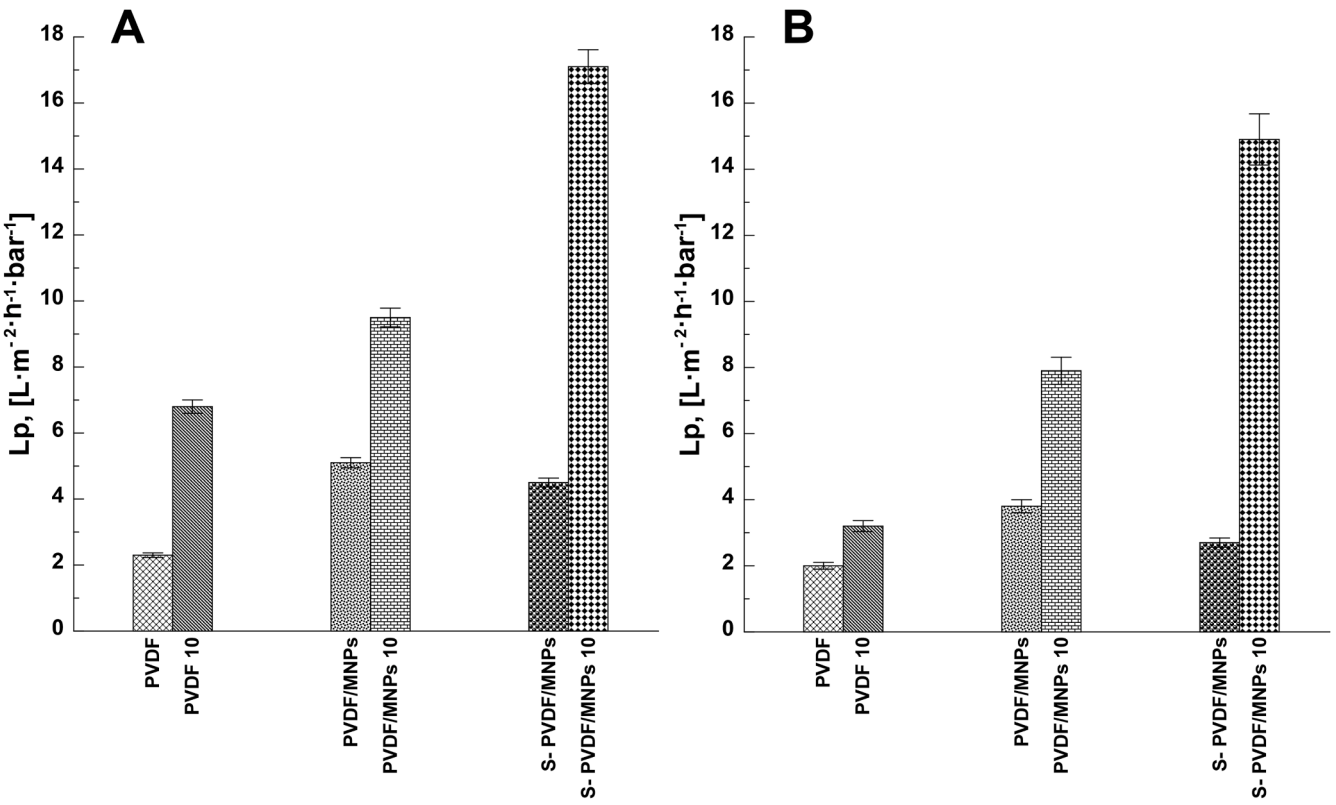

Fig. 8. Membrane permeability with pure water (A) and 0.1 wt % solution of polyacrylic acid (B).

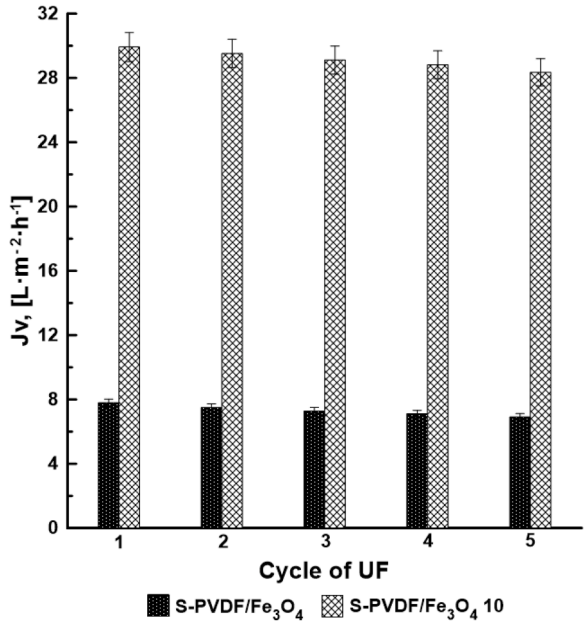

Fig. 9. Permeate fluxes of S-PVDF/Fe_3O_4 and S-PVDF/Fe_3O_4 10 membranes over 5 cycles of UF: Δ P of 2 bar; 0.1 wt % solution of PAA.

polymeric matrix. On the other hand, the cationic nature of polyethyleneimine grafted to the membrane surface greatly influenced the value of IEP (7.7 ± 0.2 mV for S-PVDF/Fe_3O_4).

3.3. Membrane morphology

Surface and cross-section microphotographs of membranes were acquired to study the morphology changes after the modification processes. According to the SEM images (Fig. 5), the original PVDF membranes possess a homogeneous flat and smooth surface. The cross-section images of the investigated membranes demonstrate the typical asymmetric microstructure of PVDF with a top skin layer, macro finger-like pores, and a dense "sponge-like" structure. Moreover, owing to the obtained SEM images, the increase of IET from 0 to 10 min in the membrane fabrication resulted in significantly changed membrane morphology, as the pore size of PVDF membrane formed with IET of 10 min was bigger than the pore size of PVDF membrane without additional IET (Fig. 5 A1 and B1). Yadav et al. [56] investigated optimal conditions for the fabrication of PVDF-TiO_2 flat sheet hydrophobic membranes. The operation parameters assessed during the membrane formation process included polymer concentration, TiO_2 concentration, evaporation time, and ethanol concentration in the coagulation bath. It was concluded that porosity showed an inverse relationship with polymer concentration, whereas TiO_2 concentration, IET, and coagulation bath concentration had a combined effect on the porosity. The optimal process parameters were determined as 16.0 wt % of polymer concentration, 1.676 wt % of TiO_2 content, and IET of 29.09 min for the PVDF membrane with desired parameters (WCA was 109° ± 2°, membrane porosity was 59.9 ± 2 %, and tensile strength was 78.7 ± 1 MPa).

As can be concluded from the SEM images (Fig. 5 C1 and D1), it can be clearly observed that adding Fe_3O_4 to the membrane matrix has a great influence on the porous structure of the membranes. Comparing microphotographs of PVDF/ Fe_3O_4 membranes with the original PVDF membranes, more macropores were observed in the structure of PVDF/ Fe_3O_4 membranes. This phenomenon can be caused by the acceleration of the exchange rate between solvent and nonsolvent materials during the membrane formation as a result of Fe_3O_4 addition [36]. Moreover, agglomerated magnetite nanoparticles were observed in the membrane matrix of PVDF/Fe_3O_4 after the modification.

Furthermore, the surface modification with polyethyleneimine and Fe_3O_4 led to the visible changes in the membrane morphology. As is

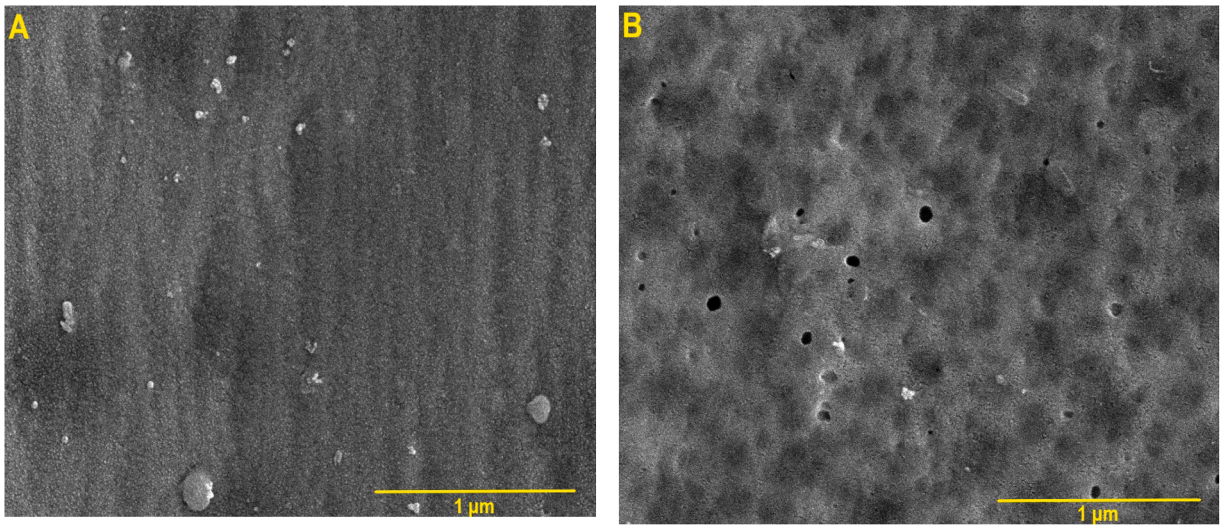

Fig. 10. Top microphotographs of: (A) – S-PVDF/Fe_3O_4; (B) – S-PVDF/Fe_3O_4 10 after cycle experiments.

Table 5
Fe^{2+} concentration in water after enhanced UF with polyacrylic acid.

C (PAA), [wt %]	C (Fe^{2+}) in permeate, [mg·L^{-1}]					
	PVDF	PVDF IET (10min)	PVDF/ Fe_3O_4	PVDF/ Fe_3O_4 IET (10 min)	S-PVDF/ Fe_3O_4	S-PVDF/ Fe_3O_4 IET (10 min)
0.1	2.81	5.68	2.96	8.45	1.13	3.41
0.3	0.80	2.69	1.13	2.96	0.11	0.59
0.5	0.65	1.10	1.01	1.31	0.08	0.24

demonstrated in Fig. 5 (E1 and F1), a high density of immobilized nanoparticles was identified on the surface of S-PVDF/Fe_3O_4. It is additional evidence of the successful attachment of the nanoparticles on the grafted PEI as a polymer linker. Significantly, the surface modification leads to a clear reduction in membrane pore size. This reduction is linked to polyethyleneimine's ability to bond to the membrane surface while simultaneously decreasing the effective pore radius.

EDX analyzes were employed to investigate the elemental existence. Fig. 6. depicts the presence of carbon, fluorine, and oxygen for the original PVDF. As expected, doping the membrane with Fe_3O_4 caused the appearance of iron in the membrane structure. The highest content of iron was determined for S-PVDF/Fe_3O_4; it can be related to the extra attachment of nanoparticles to the membrane surface, which was also confirmed by SEM (Fig. 5).

The topography of the PVDF, PVDF/Fe_3O_4, and S-PVDF/Fe_3O_4 membranes are presented in Fig. 7, representing AFM images of the analyzed samples. Notably, the bright areas represent the highest points of the membrane surface, while the dark areas indicate the presence of valleys and pores. According to Table 4, the original PVDF and PVDF 10 were characterized by the lowest root mean square (RMS) roughness values (26.7 ± 0.3 nm and 28.7 ± 0.3 nm respectively). Doping of the PVDF matrix with magnetite nanoparticles increased the RMS values by 9–12 % (30.4 ± 0.3 nm for PVDF/Fe_3O_4 and 31.3 ± 0.3 nm for PVDF/Fe_3O_4 10). Generally, increased surface roughness causes improved permeability, whereas increased fouling is also associated with a higher RMS [57,58]. The highest RMS (54.2 ± 0.3 and 46.5 ± 0.3 nm) were characteristic of modified PVDF membranes without and with evaporation time, respectively. The reason is the successful immobilization of Fe_3O_4 nanoparticles on the membrane surface. It should be noted that the presence of sphere-like particles (size in the range of 70 – 250 nm) is visible in Fig. 7E and F.

3.4. Enhanced Fe^{2+} ions removal

The volumetric flow is an important parameter for estimating the transport properties of the membrane in the process of UF. The dependences of the flow of the applied pressure were obtained to determine the hydrodynamic permeability coefficient for fabricated PVDF membranes. The values of the hydrodynamic water permeability coefficient are presented in Fig. 8. In general, the fabricated PVDF membranes showed an upward trend of Lp value with increasing evaporation time. Compared with a PVDF membrane without evaporation time, a PVDF membrane with an IET of 10 min demonstrated a higher Lp value (2.3 LMH·bar^{-1} vs 6.8 LMH·bar^{-1}). Membranes formed with Fe_3O_4 nanoparticles were characterized by increased Lp values compared to the pristine PVDF membranes (5.1 LMH·bar^{-1} and 9.5 LMH·bar^{-1}, respectively). The highest value of the hydrodynamic permeability coefficient was shown by S-PVDF/Fe_3O_4 with IET of 10 min (17.1 LMH·bar^{-1}). The 152 % increase in Lp value compared with the original PVDF 10 can be explained by the hydrophilization of the membrane surface after modification and doping of the membrane matrix with Fe_3O_4.

For the full and systematic characterization of the transport properties across the prepared membranes during the enhanced ultrafiltration process, membrane permeability values were determined using 0.1 wt % of polyacrylic acid (Fig. 8B). According to the obtained results, a decrease in the membrane permeability with PAA was observed. S-PVDF/Fe_3O_4 with IET of 10 min was characterized by the lowest differences (13 %) between water membrane permeability and membrane permeability with PAA. The observed small change in the Lp values was consistent with the presence and rotation of the magnetite nanoparticles in the boundary layer, making it possible to reduce concentration polarization and fouling phenomena during the UF.

To assess the stability and the reusability of the PVDF membranes with immobilized magnetite nanoparticles, 5 successive cycles of UF were performed in the dead-end mode under the pressure of 2 bar and the magnetic stirring of 250 rpm. The duration of each cycle was equal to 2 h. The 0.1 wt % solution of polyacrylic acid was used as a model compound to evaluate the permeate flux of the investigated membranes. As can be seen in Fig. 9, Jv values practically did not change during UF experiments. Flux values of S-PVDF/Fe_3O_4 and S-PVDF/Fe_3O_4 10 declined by 11 and 5 % during 10 h of the process. The morphology of S-PVDF/Fe_3O_4 and S-PVDF/Fe_3O_4 10 after cycle experiments were presented in Fig. 10.

The rejection of iron (II) ions was also determined in the process of PAA-enhanced ultrafiltration. The results of the experiments using

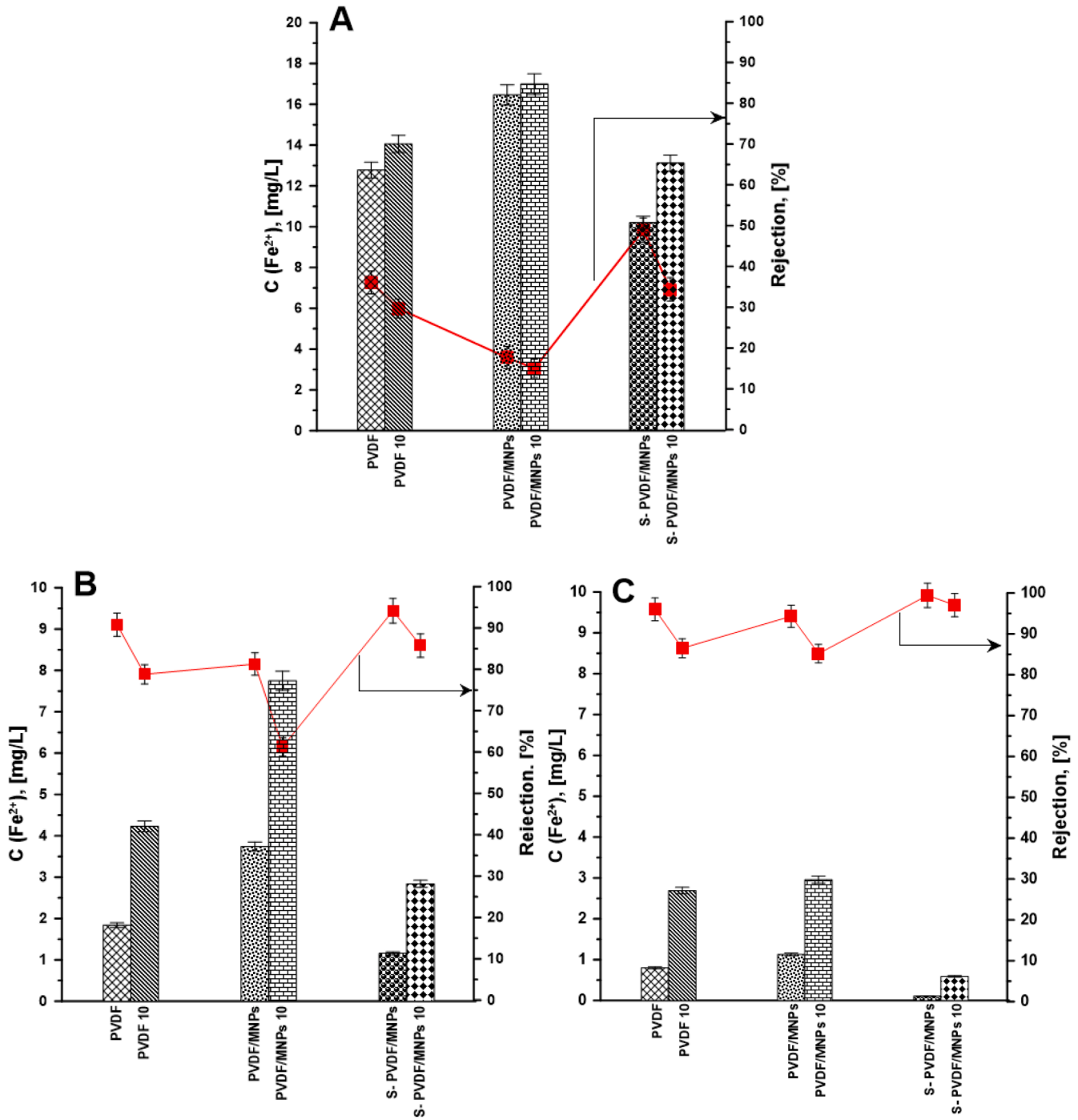

Fig. 11. Iron concentration in permeate and rejection after enhanced ultrafiltration with 0.3 wt % of polyacrylic acid at different pH values: (A) pH = 4; (B) pH = 6; (C) pH = 8.

solutions with different content of PAA (0.1, 0.3, and 0.5 wt %) are shown in Table 5. It was confirmed that the PVDF membrane with immobilized Fe_3O_4 demonstrated the best ability for Fe^{2+} removal. Namely, utilizing the S-PVDF/Fe_3O_4 with IET of 10 min resulted in the concentration of Fe^{2+} in the permeate of 3.41 mg·L^{-1}. Moreover, the content of iron (II) ions was equal to 1.13 mg·L^{-1} for the S-PVDF/Fe_3O_4 membrane without IET. Furthermore, the separation efficiency of the enhanced UF increased with the concentration of PAA. Comparing experiments with 0.1 wt %, 0.3 wt %, and 0.5 wt % of PAA, the iron (II) contents were 1.13 mg·L^{-1}, 0.11 mg·L^{-1}, and 0.08 mg·L^{-1} for S-PVDF/Fe_3O_4. This tendency was related to a higher degree of iron (II) ions binding with polyacrylic acid.

Taking into account better separation efficiency, further experiments were conducted with water solutions of PAA with concentrations of 0.3 and 0.5 wt %. The results of the study are shown in Figs. 11 and 12, respectively. The rejection values of Fe^{2+} were also evaluated at different pH values (4, 6, and 8). The best separation features were observed for all the investigated membranes at a pH value equal to 8. Ultrafiltration carried out at pH 4.0 led to the reduction of the efficiency of iron removal by 35–58 %. It can be explained by a reversible conformational change (coil-to-globule transition) of polyacrylic acid at a pH value of around 5.0 that is driven by the level of ionization of the carboxylic group [59]:

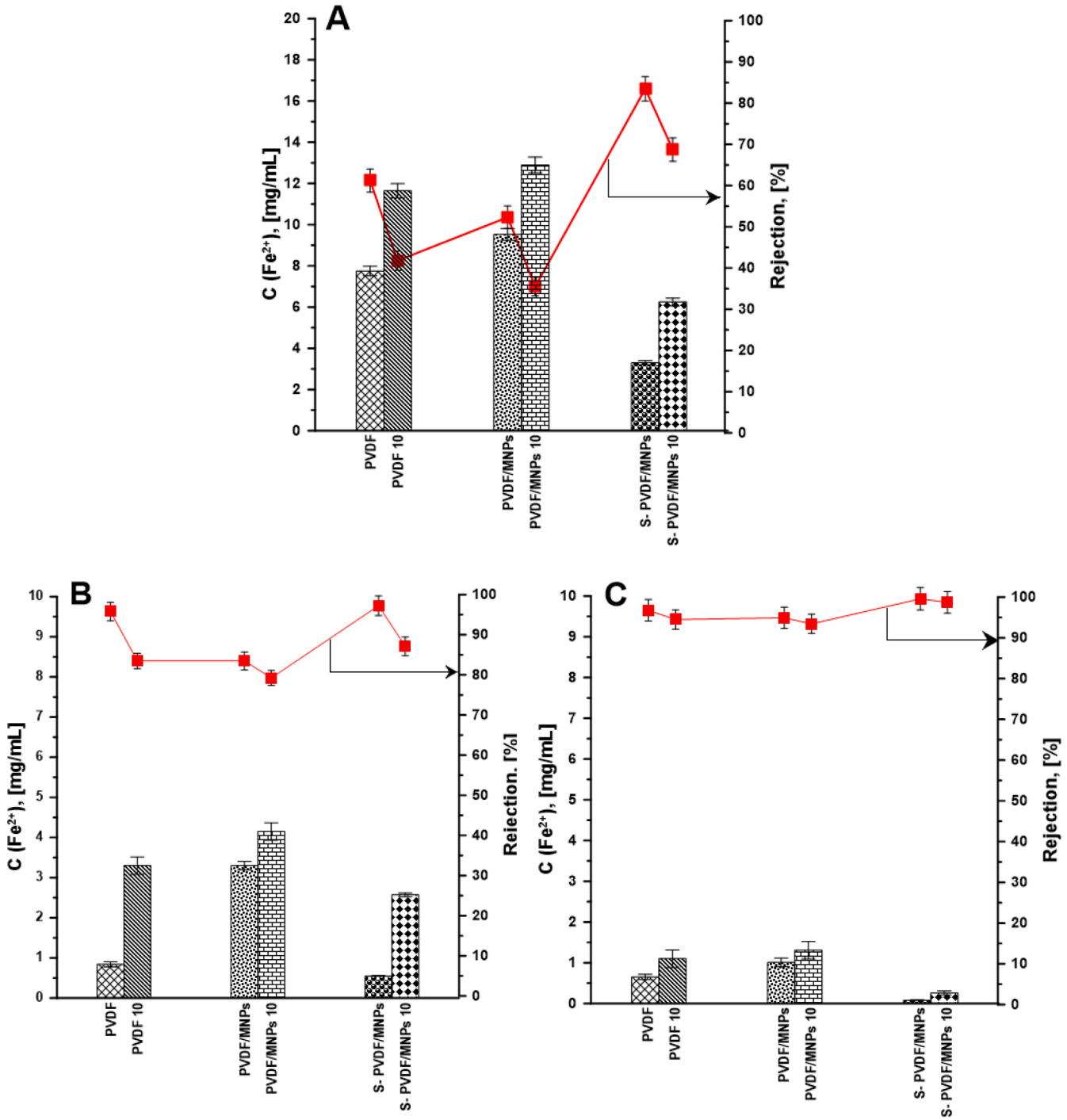

Fig. 12. Iron concentration in permeate and rejection after enhanced ultrafiltration with 0.5 wt % of polyacrylic acid at different pH values: (A) pH = 4; (B) pH = 6; (C) pH = 8.

$$RCOOH \leftrightarrow H^{+} + RCOO^{-} \quad (6)$$

At the low pH range, PAA adopts a compact (but not fully collapsed) globular conformation, allowing it to pass easily through membranes [60]. Moreover, the membrane streaming potential had to be taken into account (Fig. 4B, Table 3). Obviously, the membrane surface carries a positive charge when the pH is below the isoelectric point, while it becomes negatively charged when the pH is above the isoelectric point. Thus, higher rejection values at higher pH can be related to the electrostatic repulsions between polyacrylic acid and membrane surface.

4. Conclusion

In the presented work, the pristine PVDF membranes and their modified derivatives were developed. Magnetite nanoparticles (Fe_3O_4) were incorporated into the PVDF membranes matrix, while there was a further surface modification with polyethyleneimine as a linker. The surface characteristics of developed membranes were assessed using SEM, IR, AFM, WCA, and zeta potential analyzes. Undoubtedly, surface modification with PEI as polycation and hydrophilic agent resulted in the hydrophilization of the membrane (WCA decreased from 106.1 ± 3 to 74.8 ± 2), and changes in isoelectric point of PVDF membrane (from

3.5 ± 0.2 to 7.7 ± 0.2).

In addition, membranes were tested using the dead-end ultrafiltration process and discussed in terms of iron removal from water using a polyelectrolyte-enhanced UF process with polyacrylic acid. Notably, PVDF with attached Fe_3O_4 and IET of 10 min possessed the highest permeability (17.1 LMH·bar^{-1}), which is 3.7 times higher compared with a similar membrane without IET. Furthermore, comparing S-PVDF/Fe_3O_4 with pristine PVDF membrane, the permeability was enhanced by 152 %. According to the high rejection values (97.1 – 99.4 %), and amount of iron in the permeate (0.08 and 0.11 mg·L^{-1}) after PAA-enhancement of UF, the potential use of PVDF membranes enhanced with Fe_3O_4 nanoparticles for the removal of Fe^{2+} excess was proven. An optimal amount of PAA and pH of solution for the removal of excess of ferrous iron from water have also been determined (0.5 wt % of PAA and pH = 8).

CRediT authorship contribution statement

Halyna Bubela: Writing – review & editing, Writing – original draft, Visualization, Validation, Methodology, Investigation, Formal analysis, Data curation, Conceptualization. **Viktoriia Konovalova:** Writing – review & editing, Supervision, Methodology, Conceptualization. **Joanna Kujawa:** Writing – review & editing, Visualization, Methodology, Formal analysis, Conceptualization. **Wojciech Kujawski:** Writing – review & editing, Supervision, Project administration, Funding acquisition.

Declaration of competing interest

The authors declare that they have no known competing financial interests or personal relationships that could have appeared to influence the work reported in this paper.

Data availability

Data will be made available on request.

References

[1] R. Zeidan, S. Min Han, C. Leeuwenburgh, R. Xiao, Iron homeostasis and organismal aging, Ageing Res. Rev. 72 (2021) 101510, https://doi.org/10.1016/j.arr.2021.101510.

[2] S. Dey, A. Sreenivasulu, G. Veerendra, A. Phani Manoj, N. Haripavan, Synthesis and characterization of mango leaves biosorbents for removal of iron and phosphorous from contaminated water, Appl. Surf. Sci. 11 (2022) 100292, https://doi.org/10.1016/j.apsadv.2022.100292.

[3] A. Basem, D. Jasim, H. Majdi, R. Mohammed, M. Ahmed, A. Al-Rubaye, E. Kianfar, Adsorption of heavy metals from wastewater by chitosan: a review, Result. Eng. 23 (2024) 102404, https://doi.org/10.1016/j.rineng.2024.102404.

[4] S. Chaturvedi, P. Dave, Removal of iron for safe drinking water, Desalination 303 (2012) 1–11, https://doi.org/10.1016/j.desal.2012.07.003.

[5] S. Dey, N. Kotaru, G. Veerendra, A. Sambangi, The removal of iron from synthetic by the applications of plants leaf biosorbents, Clean. Eng. Technol. 9 (2022) 100530, https://doi.org/10.1016/j.clet.2022.100530.

[6] Guidelines For Drinking-Water Quality, 4th edition, World Health Organization, 2017. ISBN: 978-92-4-154995-0.

[7] Directive (EU). 2020/2184 of the European Parliament and of the Council of 16th December 2020 on the quality of water intended for human consumption, 2020.

[8] K. Norherdawati, M. Abdul Wahab, A. Siti Rozaimah Sheikh, Performance of membrane filtration in the removal of iron and manganese from Malaysia's groundwater, Membr. Water Treat. 7 (2016) 277–296, https://doi.org/10.12989/mwt.2016.7.4.277.

[9] R. Fakhtekh, E. Chabanon, D. Mangin, R. Ben Amar, C. Charcosset, Removal of iron using an oxidation and ceramic microfiltration hybrid process for drinking water treatment, Desalinat. Water Treat 66 (2017) 210–220, https://doi.org/10.5004/dwt.2017.20225.

[10] G. Türkoğlu Demirkol, S. Özden Çelik, S. Güneş Durak, S. Acarer, E. Çetin, S. Akarçay Demir, N. Tüfekci, Effects of $Fe(OH)_3$ and MnO_2 flocs on iron/manganese removal and fouling in aerated submerged membrane systems, Polym. (Basel) 13 (2021) 3201, https://doi.org/10.3390/polym13193201.

[11] G. Kang, Y. Cao, Application and modification of poly(vinylidene fluoride) (PVDF) membranes – a review, J. Membr. Sci. 463 (2014) 145–165, https://doi.org/10.1016/j.memsci.2014.03.055.

[12] S. Karki, G. Hazarika, D. Yadav, P. Ingole, Polymeric membranes for industrial applications: recent progress, challenges and perspectives, Desalination 573 (2024) 117200, https://doi.org/10.1016/j.desal.2023.117200.

[13] Y. Ibrahim, V. Naddeo, F. Banat, S. Hasan, Preparation of novel polyvinylidene fluoride (PVDF) – Tin (IV) oxide (SnO_2) ion exchange mixed matrix membranes for the removal of heavy metal ions, Sep. Purif. Technol. 250 (2020) 117250, https://doi.org/10.1016/j.seppur.2020.117250.

[14] H. Zhao, D. Zhang, H. Sun, Y. Zhao, M. Xie, Adsorption and detection of heavy metals from aqueous water by PVDF/ATP-CDs composite membrane, Colloid. Surf. A Physicochem. Eng. Asp. 641 (2022) 128573, https://doi.org/10.1016/j.colsurfa.2022.128573.

[15] S. Mishra, A. Singh, J. Singh, Ferrous sulfide and carboxyl-functionalized ferroferric oxide incorporated PVDF-based nanocomposite membranes for simultaneous removal of highly toxic heavy-metal ions from industrial ground water, J. Membr. Sci. 593 (2020) 1174222, https://doi.org/10.1016/j.memsci.2019.117422.

[16] E. Abdulkarem, Y. Ibrahim, M. Kumar, H. Arafat, V. Naddeo, F. Banat, S. Hasan, Polyvinylidene fluoride (PVDF)-α-zirconium phosphate (α-ZrP) nanoparticles based mixed matrix membranes for removal of heavy metal ions, Chemosphere 267 (2021) 128896, https://doi.org/10.1016/j.chemosphere.2020.128896.

[17] X. Zhao, J. Li, S. Mu, W. He, D. Zhang, X. Wu, C. Wang, H. Zeng, Efficient removal of mercury ions with MoS_2-nanosheet-decorated PVDF composite adsorption membrane, Environ. Pollut. 268 (2021) 115705, https://doi.org/10.1016/j.envpol.2020.115705.

[18] L. Teng, C. Yue, G. Zhang, Epoxied SiO_2 nanoparticles and polyethyleneimine (PEI) coated polyvinylidene fluoride (PVDF) membrane for improved oil water separation, anti-fouling, dye and heavy metal ions removal capabilities, J. Colloid. Interface Sci. 630 (2023) 416–429, https://doi.org/10.1016/j.jcis.2022.09.148.

[19] M. Pishnamazi, S. Koushkbagni, S. Samira Hosseini, M. Darabi, A. Yousefi, M. Irani, Metal organic framework nanoparticles loaded – PVDF/chitosan nanofibrous ultrafiltration membranes for the removal of BSA protein and Cr (VI) ions, J. Mol. Liq. 317 (2020) 113934, https://doi.org/10.1016/j.molliq.2020.113934.

[20] S. Du, P. Zhao, L. Wang, G. He, X. Jiang, Progresses of advanced anti-fouling membrane and membrane processes for high salinity wastewater treatment, Result. Eng. 17 (2023) 100995, https://doi.org/10.1016/j.rineng.2023.100995.

[21] J. Ren, W. Xia, X. Feng, Y. Zhao, Surface modification of PVDF membrane by sulfonated chitosan for enhanced anti-fouling via PDA coating layer, Mater. Lett. 307 (2022) 130981, https://doi.org/10.1016/j.matlet.2021.130981.

[22] G. Fan, C. Chen, X. Chen, Z. Li, S. Bao, J. Luo, D. Tang, Z. Yan, Enhancing the antifouling and rejection properties of PVDF membrane by Ag_3PO_4-GO modification, Sci. Total Environ. 801 (2021) 149611, https://doi.org/10.1016/j.scitotenv.2021.149611.

[23] S. Al-Gharabli, J. Kujawa, M. Mavukkandy, H. Arafat, Functional groups docking on PVDF membranes: novel Pirahna approach, Eur. Polym. J. 96 (2017) 414–428, https://doi.org/10.1016/j.eurpolymj.2017.09.029.

[24] E. Akin, S. Mohammad, T. Gharibzahedi, H. Qiu, A. Aliyeva, Z. Altintas, Chitosan-functionalized PVDF and PES membranes integrates by epitope-imprinted polymers for targeted hepatitis A virus capture, J. Membr. Sci. 709 (2024) 123084, https://doi.org/10.1016/j.memsci.2024.123084.

[25] V. Maggay, H. Lin, T. Abebe Gelete, Y. Chang, Y. Huang, A. Venault, 3 stage filtration system utilizing 3 distinct membranes derived from one single dope solution and finely-tuned phase inversion processes, Sep. Purif. Technol. 311 (2023) 123275, https://doi.org/10.1016/j.seppur.2023.123275.

[26] L.Hui Ting, Y. Teow, E. Mahmoudi, B. Ooi, Development and optimization of low surface free energy of rGO-PVDF mixed matrix membrane for membrane distillation, Sep. Purif. Technol. 305 (2023) 122428, https://doi.org/10.1016/j.seppur.2022.122428.

[27] T. Mar, Y. Xue, Y. Chang, Z. Yu, Z. Du, B. Cao, R. Zhang, Fabrication and performance optimization of an advanced pervaporation desalination membrane: a study utilizing PVDF and hydrophilic active layer as composite, Result. Eng. 23 (2024) 102760, https://doi.org/10.1016/j.rineng.2024.102760.

[28] L. Cao, H. Liu, H. Li, H. Lin, L. Li, Dopamine co-coating with fulvic acid on PVDF membrane surface for hydrophilicity improvement and highly-efficient oily water purification, J. Water Proc. Eng. 64 (2024) 105722, https://doi.org/10.1016/j.jwpe.2024.105722.

[29] Y. Zhang, Y. Tong, L. Shi, C. Miao, W. Li, One-step rapid co-decomposition of oxidant induced mussel-polyphenol coating on PVDF substrate for separation oily water, Sep. Purif. Technol. 303 (2022) 122304, https://doi.org/10.1016/j.seppur.2022.122304.

[30] Z. Feng, T. Wang, Y. Lin, L. Wang, Y. Tang, H. Wu, H. Chen, L. Yu, X. Wang, A facile and scalable fabrication procedure for PVDF-PDA/PEI/SiO_2 hollow fiber composite ultrafiltration membranes: integration of co-deposition and cross-linking, Result. Eng. 22 (2024) 102055, https://doi.org/10.1016/j.rineng.2024.102055.

[31] H. Wang, B. Yan, Z. Hussain, W. Wang, N. Chang, Chemically graft aminated GO onto dehydro-fluorinated PVDF for preparation of homogeneous DF-PVDF/GO-NH2 ultrafiltration membrane with high permeability and antifouling performance, Surf. Interface. 33 (2022) 102255, https://doi.org/10.1016/j.surfin.2022.102255.

[32] W. Jankowski, W. Kujawski, J. Kujawa, Enhanced performance of electrospun PVDF membranes modified with rare-earth metal oxides for membrane distillation: a systematic study, Desalination 584 (2024) 117742, https://doi.org/10.1016/j.desal.2024.117742.

[33] E. Hamad, S. Al-Gharabli, J. Kujawa, Tunable hydrophobicity and roughness on PVDF surface by grafting to mode – approach to enhance membrane performance in membrane distillation process, Sep. Purif. Technol. 291 (2022) 120935, https://doi.org/10.1016/j.seppur.2022.120935.

[34] T. Hanh Le, S. Singto, W. Sajomsang, R. Mongkolnavin, R. Nuisin, P. Painmanakul, S. Sairiam, Hydrophobic PVDF hollow fiber membrane modified with pulse inductively coupling plasma activation and chloroalkylsilanes for effective dye wastewater treatment by ozonation membrane contactor, J. Membr. Sci. 635 (2021) 119443, https://doi.org/10.1016/j.memsci.2021.119443.
[35] S. Al-Gharabli, Z. Flanc, K. Pianka, A. Terzyk, W. Kujawski, J. Kujawa, Porcupine quills-like-structures containing smart PVDF/chitosan hybrids for anti-fouling membrane applications and removal of hazardous VOCs, J. Chem. Eng. 452 (2023) 139281, https://doi.org/10.1016/j.cej.2022.139281.
[36] P. Jimenez-Meneses, M.-J. Bañuls, R. Puchades, Á. Maquieira, Novel and rapid activation of polyvinylidene fluoride membranes by UV light, React. Funct. Polym. 140 (2019) 56–61, https://doi.org/10.1016/j.reactfunctpolym.2019.04.012.
[37] B. Li, M. Meng, Y. Cui, Y. Wu, Y. Zhang, H. Dong, Z. Zhu, Y. Feng, C. Wu, Changing conventional blending photocatalytic membranes (BPMs): focus on improving photocatalytic performance of Fe_3O_4/g-C_3N_4/PVDF membranes through magnetically induced freezing casting method, J. Chem. Eng 365 (2019) 405–414, https://doi.org/10.1016/j.cej.2019.02.042.
[38] J. Sun, S. Li, Z. Ran, Y. Xiang, Preparation of Fe_3O_4@TiO_2 blended PVDF membrane by magnetic coagulation bath and its permeability and pollution resistance, J. Mater. Res. Technol. 9 (2020) 4951–4967, https://doi.org/10.1016/j.jmrt.2020.03.014.
[39] I. Koyuncu, B. Gul, M. Esmaeli, E. Pergenc, O. Teber, G. Tuncay, H. Karimi, S. Parvaz, A. Maleki, V. Vatanpour, Modification of PVDF membranes by incorporation Fe_3O_4@Xanthan gum to improve anti-fouling, anti-bacterial, and separation performance, J. Environ. Chem. Eng. 10 (2022) 107784, https://doi.org/10.1016/j.jece.2022.107784.
[40] H. Gumus, Performance investigation of Fe_3O_4 blended poly(vinylidene fluoride) membrane on filtration and benzyl alcohol oxidation: evaluation of sufficiency for catalytic reactors, Chin. J. Chem. Eng. 27 (2019) 314–321, https://doi.org/10.1016/j.cjche.2018.05.006.
[41] N. Enemuo, H. Richards, M. Daramola, Evaluation of the performance of Fe_3O_4-NPs/PVDF nanocomposite membrane for removal of BTEX from contaminated water, J. Water Proc. Eng. 60 (2024) 105185, https://doi.org/10.1016/j.jwpe.2024.105185.
[42] T. Agbaje, S. Al-Gharabli, M. Mavukkandy, J. Kujawa, H. Arafat, PVDF/magnetite blend membranes for enhanced flux and salt rejection in membrane distillation, Desalination 436 (2018) 69–80, https://doi.org/10.1016/j.desal.2018.02.012.
[43] V. Konovalova, I. Kolesnyk, O. Ivanenko, A. Burban, Fe^{2+} removal from water using PVDF membranes modified with magnetite nanoparticles by polyelectrolyte enhanced ultrafiltration, Environ. Prot. Eng. 21 (2018) 39–49, https://doi.org/10.17512/ios.2018.1.4.
[44] Y. Wang, Z. Guo, Y. Yang, Y. Li, Q. Guo, P. Cui, W. Li, Fabrication of magnetically responsive anti-fouling and easy-cleaning nanofiber membrane and its application for efficient oil-water emulsion separation, Chin. J. Chem. Eng. 41 (2022) 286–293, https://doi.org/10.1016/j.cjche.2021.12.013.
[45] V. Konovalova, I. Kolesnyk, A. Burban, W. Kujawski, K. Knozowska, J. Kujawa, Improvement of separation and transport performance of ultrafiltration membranes by magnetically active nanolayer, Colloid. Surf. A Physicochem. Eng. Asp. 569 (2019) 67–77, https://doi.org/10.1016/j.colsurfa.2019.02.061.
[46] H. Himstedt, Y. Qian, D. Prasad, Q. Xianghong, W. Ranil, M. Ulbricht, Magnetically activated micromixers for separation membranes, Langmuir 27 (2011) 5574–5581, https://doi.org/10.1021/la200223g.
[47] H. Himstedt, A. Sengupta, Q. Xianghong, S. Wickramasinghe, Magnetically responsive nanofiltration membranes for treatment of coal bed methane produced water, J. Taiwan Inst. Chem. Eng. 94 (2019) 97–108, https://doi.org/10.1016/j.jtice.2018.01.007.
[48] A. Rahimpour, M. Kebria, M. Firouzjaei, M. Mozafari, M. Elliot, M. Sadrzadeh, Chapter 1 – Nonsolvent-induced phase separation by phase inversion, Polym. Membr. Format. Phase Invers. (2024) 1–36, https://doi.org/10.1016/B978-0-323-95628-4.00009-4.
[49] H. Bubela, V. Konovalova, J. Kujawa, I. Kolesnyk, A. Burban, W. Kujawski, Enhancing of transport parameters and antifouling properties of PVDF membranes modified with Fe_3O_4 nanoparticles in the process of proteins fractionation, Sep. Purif. Technol. 325 (2023) 124573, https://doi.org/10.1016/j.seppur.2023.124573.
[50] G. Vitola, R. Mazzei, E. Fontananova, L. Giorno, PVDF membrane biofunctionalization by chemical grafting, J. Membr. Sci. 476 (2015) 483–489, https://doi.org/10.1016/j.memsci.2014.12.004.
[51] I. Kolesnyk, J. Kujawa, H. Bubela, V. Konovalova, A. Burban, A. Cyganiuk, W. Kujawski, Photocatalytic properties of PVDF membranes modified with g-C_3N_4 in the process of Rhodamines decomposition, Sep. Purif. Technol. 250 (2020) 117231, https://doi.org/10.1016/j.seppur.2020.117231.
[52] M. Ebrahimi, W. Kujawski, K. Fatyeyeva, Fabrication of polyamide-6 membranes – the effect of gelation time towards their morphological, physical and transport properties, Membr. (Basel) 12 (2022) 315, https://doi.org/10.3390/membranes12030315.
[53] A. Imbrogno, J. Calvo, M. Breida, R. Schwaiger, A. Schafer, Molecular weight cut off (MWCO) determination in ultra- and nanofiltration: review of methods and implications on organic matter removal, Sep. Purif. Technol. 354 (2025) 128612, https://doi.org/10.1016/j.seppur.2024.128612.
[54] T.A. Otitoju, Y. Bai, Y. Tian, Z. Feng, Y. Wang, X. Zhang, T. Sun, Surface modification of PVDF membrane via layer-by-layer self assembly of TiO_2/V for enhanced photodegradation of emerging organic pollutants and the implication for wastewater remediation, Chem. Eng. Sci. 275 (2023) 118762, https://doi.org/10.1016/j.ces.2023.118762.
[55] J. Kujawa, M. Zięba, W. Zięba, S. Al-Gharabli, W. Kujawski, A.P. Terzyk, Carbon nanohorn improved durable PVDF membranes – The future of membrane distillation and desalination, Desalination 511 (2021) 115117, https://doi.org/10.1016/j.desal.2021.115117.
[56] M. Yadav, S. Upadhyay, K. singh, Process optimization for fabrication of PVDF – TiO2 hydrophobic membrane using phase inversion method for desalination application using VMD, Mater. Today: Proc. 90 (2023) 39–50, https://doi.org/10.1016/j.matpr.2023.06.153.
[57] A.T. Yasir, A. Benamor, A.H. Hawari, Enhancement of polysulfone ultrafiltration membranes with third generation poly(amido amine)-graphene oxide nanocomposite, J. Water Proc.Eng. 54 (2023) 103991, https://doi.org/10.1016/j.jwpe.2023.103991.
[58] S.H. Woo, B.R. Min, J.S. Lee, Change of surface morphology, permeate flux, surface roughness and water contact angle for membranes with similar physicochemical characteristics (except surface roughness) during microfiltration, Sep. Purif. Technol. 187 (2017) 274–284, https://doi.org/10.1016/j.seppur.2017.06.030.
[59] T. Swift, L. Swanson, M. Geoghegan, S. Rimmer, The pH-responsive behavior of poly(acrylic acid) in aqueous solution is dependent on molar mass, Soft. Matter. 12 (2016) 2542–2549, https://doi.org/10.1039/C5SM02693H.
[60] D. Mintis, V. Mavrantzas, Effect of pH and molecular length on the structure and dynamics of short poly(acrylic acid) in dilute solution: detailed molecular dynamics study, J. Phys. Chem. 123 (2019) 4204–4219, https://doi.org/10.1021/acs.jpcb.9b01696.